A Cost-effective Wideband MIMO Channel Sounder and Initial Co-located 2.4 GHz and 5.2 GHz Measurements

B.T. Maharaj[1], L.P. Linde[1], J.W. Wallace[2], M.A. Jensen[2]

[1]University of Pretoria
Dept. of Electrical, Electronic and Computer Eng.
Lynnwood Road, Pretoria, 0002.

[2]Brigham Young University
Electrical and Computer Engineering Dept.
459 CB, Provo, UT 84602.

sunil.maharaj@up.ac.za, llinde@postino.up.ac.za, wall@ieee.org, jensen@ee.byu.edu

ABSTRACT

A cost-effective, experimental MIMO channel sounder is presented, capable of performing measurements with up to eight transmit and eight receive elements over 80 MHz of system bandwidth. The system provides the wideband channel transfer matrix for both indoor and outdoor wireless communication scenarios, allowing direct measurement of key MIMO system parameters. The system is described, fundamental hardware building blocks are outlined, and post-processing data algorithms are presented. Initial investigations on the effect of frequency scaling and array configuration at 5.2 GHz and 2.4 GHz are also presented.

1. INTRODUCTION

Pioneering work by Telatar [1] and Foschini, et al [2] on multiple-input multiple-output (MIMO) channels has shown that by employing multiple antennas at both the transmitter and receiver, one can significantly increase the capacity of the wireless channel in a scattering-rich environment without increasing system bandwidth. These MIMO systems are good candidates for wideband and ultra-wideband wireless local area networks. Research undertaken in [3]-[6] explores this opportunity to increase capacity through stochastic and geometric MIMO models.

Algorithms that achieve this increased capacity need to exploit the multipath structure by smartly coding the data in both space and time [7]. Therefore in order to assess the performance of such systems, one must gain an improved understanding of the complex spatial behavior of wireless MIMO channels [3]. Although statistical analyses [2] and ray tracing are useful for initial modeling, these tools often do not represent true channel behavior.

Although the most accurate representation of real-world channels is available by direct measurement, MIMO channel sounders are out of reach of many researchers due to the high cost. We present a flexible cost-effective wideband channel sounder that was constructed almost entirely of conventional off-the-shelf components with a total cost of approximately USD 60k, representing an order of magnitude reduction compared to some commercial systems. This sounder is able to probe microwave bands from 2 to 8 GHz using 80 MHz of instantaneous bandwidth. A switched architecture with 8 transmitters and receivers is employed to keep costs low and simplify system design and calibration.

The organization of this paper is as follows: Section 2 describes the key elements of the measurement system. Section 3 explains data processing, such as capacity computations and normalization. Section 4 presents initial measurements at 2.4 GHz and 5.2 GHz for a single indoor scenario in our measurement campaign, demonstrating the effect of frequency scaling and array configuration on capacity. Section 5 concludes the paper.

2. MEASUREMENT SYSTEM

2.1 Measurement Setup

Fig.1 depicts the transmit (TX) side of the channel probing system. The flexibility of the system allows the channel to be probed with arbitrary baseband signals (chirps, PRN sequences, etc.) For simplicity, we excited the channel with a repetitive multi-tone baseband signal that is mixed with the carrier frequency, generated very easily with a Rhode & Schwarz SMU200 vector signal generator. The multi-tone signal is of the form

$$x(t) = \sum_{i=0}^{N} \cos(2\pi f_i t + \varphi_i) \qquad (1)$$

where

$$f_i = (0.5 + i)MHz$$

$$i = 0,1,...,39$$

$$\varphi_i = \{0, \pi\}$$

and φ_i is random (but fixed) phase shift for each tone that spreads the signal energy in time. To avoid artifacts

associated with turning the signal on and off abruptly, the multitone signal of length T is multiplied by a Gaussian windowing function of the form

$$w(t) = \begin{cases} e^{-(T_1-t)^2/2\sigma^2}, & 0 \le t < T_1 \\ e^{-(T_2-t)^2/2\sigma^2}, & T_2 < t \le T \\ 1, & Otherwise \end{cases} \quad (2)$$

where T_1 and T_2 are the limits of the window, and the standard deviation σ controls the rise and fall time of the window. After power amplification, the windowed multitone signal is fed to a broadband microwave PIN diode (SP8T) switch, which routes the signal to one of N_T output antennas. The output power of the signal generator was adjusted to obtain a peak output power of 27 dBm.

Synchronization is achieved with highly stable 10MHz rubidium oscillators at TX and RX, whose careful calibration is critical to ensure negligible drift of relative TX/RX timing. RF sources were also phase locked to the rubidium references to ensure minimal frequency offset and drift. A custom designed synchronization (SYNC) unit provides all necessary triggering at TX and RX. This unit accepts the 10 MHz input reference and produces a trigger pulse on EVT1 every Q clocks and on EVT2 for every $Q \cdot N$ clocks, where N is the number of antennas. The unit also generates TTL switch signals that enable a new antenna every Q clocks. The TX/RX timing units are initially synchronized with a simple reset switch connected simultaneously to both units.

For the transmitter Q_T was set to 200 to give 20 μs of dwell-time for each transmit antenna. Combined with the Gaussian window, the channel is excited for approximately 15 μs on each antenna. Since there are N_T=8 transmit antennas, a complete scan of the array requires 160 μs. Also EVT1 is connected to the trigger input of the signal generator to ensure that the baseband signal waveform begins at the correct time instant.

Fig.2 depicts the receive system, where a SP8T switch routes the incoming signal from one of the N_R receive antennas to the receive RF chain. This signal is amplified by 40 dB though a low noise amplifier (LNA) having a noise figure (NF) of 3.5 dB, down-converted to a 50 MHz intermediate frequency (IF), filtered, and sampled at 500 Msamples/s through Channel1 of the high speed data acquisition card. Channel2 of the same card acquired the 10 MHz reference to allow accurate re-sampling of the received waveforms to ensure complete phase-coherence of the system.

At the receiver, Q_R was set to 1600, thus causing a single transmit antenna switch for each complete scan of the transmit array. With N_R=8 receive antennas, a complete scan of the MIMO channel required 1.28 ms. EVT2 of the receive SYNC unit is attached to the trigger of the acquisition card, ensuring that sampling is performed over the correct window of time.

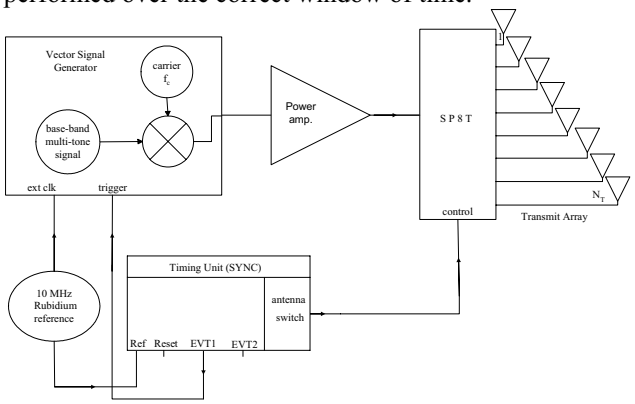

Fig. 1 High level TX system diagram of wideband MIMO channel sounder

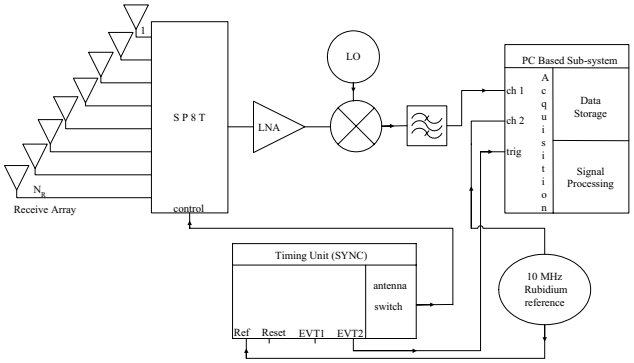

Fig. 2 High level RX system diagram of wideband MIMO channel sounder

The wideband MIMO channel response **H**(ω) for the *j*th TX and *i*th RX is computed at K=80 discrete frequency bins by dividing the FFT of the measured signal on the *j*th TX and *i*th RX timeslot by the FFT of the known transmit waveform and selecting bins corresponding to the tones. Proper choice of the waveform length ensures that each tone frequency coincides with a single FFT bin.

2.2 Measurement Environment

The measurements reported herein were carried out in the offices and laboratories at the Carl Emily Fuchs Institute of Microelectronic (CEFIM) in the Department of Electrical, Electronic and Computer Engineering at the University of Pretoria, South Africa. TX was located at the same fixed position in the corridor, while the RX antenna was located in 10 different adjoining offices and laboratories. Two antenna types were employed in the measurement: (1) linear dual-polarized patch arrays with λ/2 inter-element spacing and (2) circular/linear vertically polarized monopole arrays with λ/2 inter-element spacing. Due to the large size of the linear dipole array at 2.4 GHz, the inter-element spacing was reduced to 0.3λ.

Measurements were taken at both 5.2 GHz and 2.4 GHz at exactly the same spot for all the locations. The internal structure of the building is largely comprised of dry wall partitioning with concrete pillars support. The locations would sufficiently resemble a rich scattering environment with wood, metallic, plants, persons and fabric make-up.

3. DATA PROCESSING

3.1 System Calibration

If the system response is known, its effect can be removed from the measured channel matrices by simple division, which process we refer to as system calibration. The system response is characterized by measuring (1) the insertion loss and phase of the SP8T switches for all 8 ports and (2) the combined response of the TX and RX RF chains when excited with the channel probing signal.

The SP8T insertion loss and phase were measured for all eight ports on a network analyzer. The combined effect of the baseband signal and TX and RX RF chains is obtained by connecting the output of the TX RF chain through the appropriate attenuators directly to the input of the receive RF chain. Since we employed an IF variable gain amplifier (VGA) that had slightly different frequency response for the various gain levels, the chain response was measured for each allowed gain level ranging from 0 to 40 dB in 5 dB steps.

3.2 Channel Matrix Evaluation

At each location, 20 channel snapshots were taken at the rate of one snapshot every 200 ms. Since the TX and RX were stationary during each measurement, very little change was noticed over this 4s acquisition time. To remove the effect of path loss in our computations, channel matrices were normalized according to

$$\widetilde{\mathbf{H}}^{(n)} = \left(\frac{1}{N_R N_T N_S} \sum_{m=1}^{N_S} \left\| \mathbf{H}^{(m)} \right\|_F^2 \right)^{-1/2} \mathbf{H}^{(n)}, \tag{3}$$

where $\widetilde{\mathbf{H}}^{(n)}$ and $\mathbf{H}^{(n)}$ are the nth normalized and non-normalized channel matrices, respectively, N_S is the number of channel measurements (snapshots and frequency bins) at a single location, and $\|\cdot\|_F$ is the Frobenius norm.

Channel capacity is computed according to the uninformed transmit capacity from [2] as

$$C = \log_2 \det(I + \frac{\rho}{N_T} \widetilde{\mathrm{H}}\, \widetilde{\mathrm{H}}^H), \tag{4}$$

where I is the 8×8 identity matrix, ρ is the average SISO SNR, $\widetilde{\mathrm{H}}$ is a normalized channel matrix, and $(.)^H$ is the conjugate matrix transpose. Eigenvalues of the channel are computed as the squares of the singular values of $\widetilde{\mathrm{H}}$.

4. INITIAL MEASUREMENT RESULTS

As an example of the capabilities of the measurement system, we present some initial data from our indoor measurements. Since the complexity of algorithms for MIMO systems will depend on the channel rank available, it is of interest to know how much this rank depends on the target center frequency and array configuration for the system. We investigated this dependence by plotting the cumulative distribution functions (cdfs) of the channel eigenvalues over all frequency bins and all measurement locations. Here we compare the distributions at 2.4 GHz with those at 5.2 GHz, as depicted in Fig. 3 for linear monopole arrays and Fig. 4 for circular monopole arrays.

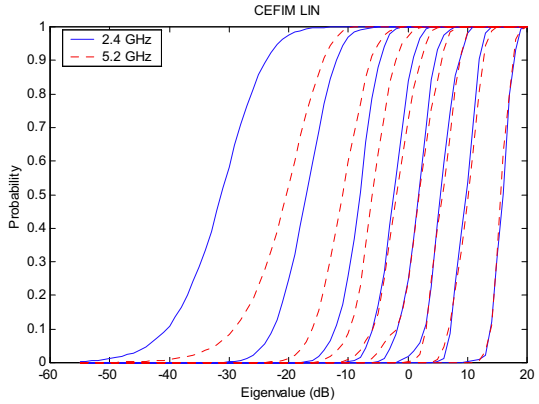

Fig. 3: Eigenvalue cdfs for linear arrays at 2.4 GHz and 5.2 GHz

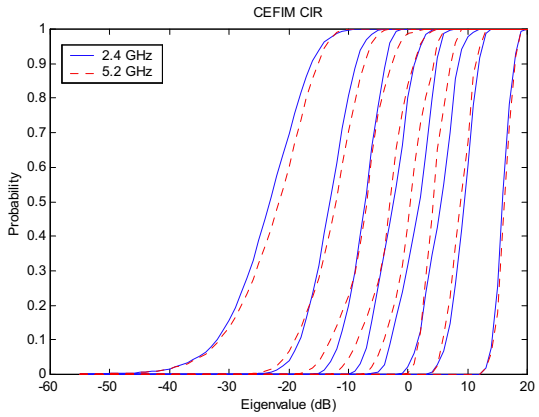

Fig. 4: Channel eigenvalue cdfs for circular arrays at 2.4 GHz and 5.2 GHz

Overall, these plots show fairly weak dependence of the eigenvalue distributions on the carrier frequency for all of the array configurations, especially for the dominant eigenvalues. Thus, from a system design standpoint, the same MIMO coding techniques will be equally applicable

to 2.4 and 5.2 GHz. This result also suggests that statistical channel models that match bulk eigenvalue behavior of data at 2.4 GHz can also be used at 5.2 GHz.

Next, we demonstrate the effect of the antenna array configuration on capacity. Fig. 5 and Fig. 6 depict the capacity probability density functions (pdfs) at 2.4 GHz and 5.2 GHz, respectively, for the 8×8 system, assuming an average SISO SNR of 20 dB. The plots demonstrate that the average capacity is only weakly affected by the array configuration.

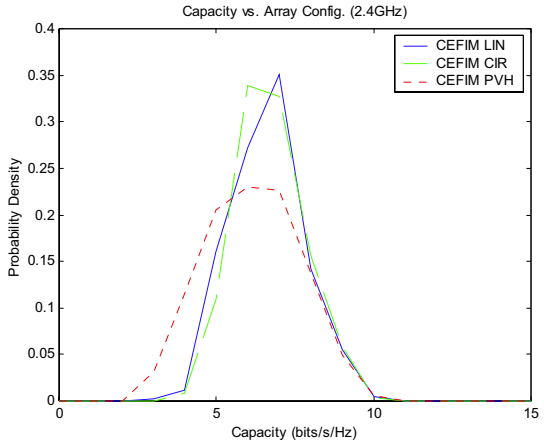

Fig. 5: Capacity pdf for the MIMO system at 2.4 GHz for the three array configurations

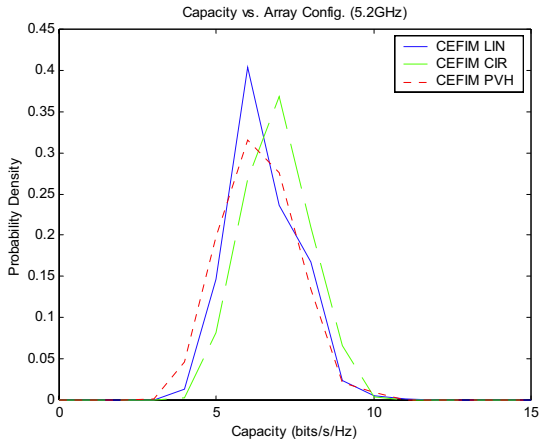

Fig. 6: Capacity pdf for the MIMO system at 5.2 GHz for the three array configurations

5. CONCLUSION

This paper has presented a flexible, low-cost MIMO channel sounder cable of probing both the 2.4 GHz and 5.2 GHz bands with 80 MHz bandwidth. With the exception of the synchronization unit, the system is constructed from off-the-shelf components. Initial co-located measurements at 2.4 GHz and 5.2 GHz indicate fairly weak dependence of bulk statistics like eigenvalue and capacity distributions on the center frequency and array type, suggesting that similar architectures are applicable to the different bands and array types. In the future, we plan to analyze this data in greater detail to develop modeling strategies that apply to both the 2.4 and 5.2 GHz bands. Our goals include data collection and model development for outdoor scenarios as well. We feel that this work will lead to a unified modeling strategy that will greatly aid MIMO system assessment and development.

6. ACKNOWLEDGEMENT

The authors would like to thank the National Research Foundation (NRF), Thuthuka Program for the financial support through GUN No. 2053857 and the Centre for Electromagnetism for the measurements at their indoor compact antenna range.

7. REFERENCES

[1] I. E. Telatar, "Capacity of multi-antenna Gaussian Channels," Technical Report #BL0112170-950615-07TM, AT&T Bell Laboratories, 1995.

[2] G. J. Foschini and M. J. Gans, "On limits of wireless communications in a fading environment when using multiple antennas," *Wireless Personal Communications*, vol. 6, no. 3, pp. 311 – 335, Kluwer Academic Publishers, March, 1998.

[3] J.W. Wallace, M.A. Jensen, A.L. Swindelhurst and B.J. Jeffs, "Experimental Characterization of the MIMO Wireless Channel: Data Acquisition and Analysis," *IEEE Trans. on Wireless Comms*., vol. 2, no. 2, pp. 335-343, March, 2003.

[4] D. Gesbert, H. Bolcskei, D. Gore and A. Paulraj, "MIMO wireless channels: Capacity and Performance prediction," *Proceedings of IEEE Globecom Conference*, vol. 2, pp. 1083-1088, November, 2000.

[5] B.T. Maharaj and L.P. Linde, "Capacity for Spatial-Temporal Correlated MIMO Fading Channel," *in Proc. IEEE Africon'04*, September, 2004.

[6] H. Ozcelik, M. Heredin, H. Hofsetter, E. Bonek, "A comparison of measured 8X8 MIMO systems with a popular stochastic channel model at 5.2 GHz," *in Proc. ICT'2003*, March, 2003.

[7] V. Tarokh, N. Seshadri and A.R. Calderbank, "Space-time codes for high data rate wireless communication: Performance criterion and code construction," *IEEE Trans. Inform. Theory*, vol. 44, pp. 744-765, March, 1998.

[8] W.C. Jakes, *Microwave Mobile Communications*. Piscataway, NJ: IEEE Press, 1993.